

Generative diffusion model for surface structure discovery

Nikolaj Rønne,¹ Alán Aspuru-Guzik,^{2,3,4,5,6} and Bjørk Hammer¹

¹*Center for Interstellar Catalysis, Department of Physics and Astronomy, Aarhus University, DK-8000 Aarhus, Denmark*

²*Department of Chemistry, University of Toronto, Toronto, Ontario, M5S 3H6, Canada.*

³*Department of Computer Science, University of Toronto, Toronto, Ontario, M5S 2E4, Canada.*

⁴*Vector Institute for Artificial Intelligence, Toronto, Ontario, M5G 1M1, Canada.*

⁵*Acceleration Consortium, Toronto, Ontario, M5S 3H6, Canada*

⁶*Canadian Institute for Advanced Research, Toronto, Ontario, M5G 1M1, Canada*

(Dated: February 28, 2024)

We present a generative diffusion model specifically tailored to the discovery of surface structures. The generative model takes into account substrate registry and periodicity by including masked atoms and z -directional confinement. Using a rotational equivariant neural network architecture, we design a method that trains a denoiser-network for diffusion alongside a force-field for guided sampling of low-energy surface phases. An effective data-augmentation scheme for training the denoiser-network is proposed to scale generation far beyond training data sizes. We showcase the generative model by investigating silver-oxide phases on Ag(111) where we are able to rediscover the “Ag₆ model” of $p(4 \times 4)\text{O}/\text{Ag}(111)$ that took scientist years to uncover by means of human intuition.

The discovery of new stable and functional materials is a prerequisite in future technological advancements in fields such as catalysis, drug discovery, carbon-capture and energy storage.[1] The design-space of stable atomistic materials is governed by quantum mechanics and it is both vast and highly complex. Generative diffusion models have proven highly capable of tackling the similarly vast design-space of images and are therefore proposed to be a natural extension to ab-initio methods for materials discovery.

The use of generative modeling in materials science has seen rapid development in recent years by utilizing variational autoencoders[2–7], generative adversarial networks[8–11], autoregressive models[12–14], reinforcement learning[15–20], language models[21–23], normalizing flows[24–27] and diffusion models[28–39]. Most developments have been in the regime of *molecular* materials with fewer generative methods tackling the more complicated case of *periodic* materials. Previous work on generative diffusion modeling of *periodic* materials has focused either on foundation models for discovery of bulk structures[28, 31, 33, 35] or discovery of mono-layer materials with no support[30, 36]. The fundamental work by Xie et al.[28], tackling bulk material generation, uses a diffusion model as the decoder in a variational autoencoder to address the inversion problem in materials discovery. A prerequisite for these developments in generative modeling of *periodic* materials is the evolution of equivariant machine learning force-fields (MLFF)[40–43]. These network architectures are able to fully capture the symmetries of *periodic* materials in 3D and open the possibility to design equivariant score-based diffusion models by utilizing the vectorial atom embeddings to predict vectorial scores.

In this work, we combine these developments and introduce a generative diffusion method for material discov-

ery specifically tailored to surface supported thin-films by including masked substrate atoms and a z -directional confinement. Furthermore, we introduce a force-field-guidance framework for sampling by introducing learned atomic forces into the sampling process and an effective data-augmentation technique to improve model stability for larger systems. We show the importance of training data selection by comparing generated materials to materials found through full density functional theory (DFT) based random structure search (RSS)[44], and finally we show the importance of the number of diffusion sampling steps on generation quality.

Generative modeling aims to allow sampling from an underlying and unknown data distribution which in the case of materials is comprised of the complicated bonding patterns of atomistic systems. Diffusion models solve this by learning the score function given as the derivative of the log-transformed data probability distribution. Hereby, a diffusion model is able to reverse a corruption process described by a stochastic differential equation (SDE) by following the reversed SDE utilizing the learned score function through a number of sampling steps.[45]

A periodic material is fully described by $\mathcal{M} = (\mathbf{z}, \mathbf{R}, \mathbf{S})$ representing the atomic types, atomic positions and periodic cell. In this work, we keep atomic types and cell fixed through the diffusion process. We define a forward diffusion process acting on the atomic positions through a SDE as

$$d\mathcal{M} = -\frac{1}{2}\beta(t)\mathcal{M}dt + \sqrt{\beta(t)}d\mathcal{W}, \quad (1)$$

where $\beta(t) = \beta_{\min} + t(\beta_{\max} - \beta_{\min})$ is a linearly increasing function between β_{\min} and β_{\max} and $d\mathcal{W}$ is infinitesimal Brownian noise.[45] The coefficient in the first term is typically called the *drift* coefficient, whereas the coefficient in the last term is known as the *diffusion* coefficient. The forward diffusion process is analytical and

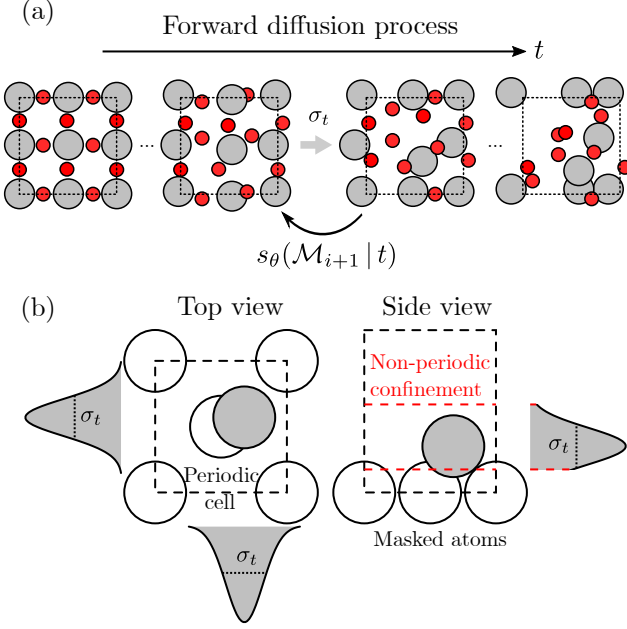


FIG. 1. (a) Schematic of the forward diffusion process where Gaussian noise, σ_t , is added at each step. At the final step the atomic positions correspond to being drawn from a uniform distribution. The denoiser-network, $s_\theta(\mathcal{M}|t)$, learns to predict the added noise at any given time-step t . (b) Side and top view of an atomistic material showing the periodic cell and the non-periodic confinement. The Gaussian distributions for perturbing the atom positions are illustrated. Light grey atoms represent masked substrate atoms whereas dark grey atoms represent atoms that are allowed to diffuse.

can be discretized and sampled. We index the discretized diffusion process by a time variable, which together with a known noise distribution allows a direct forward sampling of noisy materials. Intuitively the SDE represents the iterative addition of Gaussian noise with variance σ_t to the atomic positions as illustrated in Fig. 1(a). The reversed diffusion process can also be formulated as a SDE and is given as

$$d\mathcal{M} = \left[-\frac{1}{2}\beta(t)\mathcal{M} - \beta(t)s(\mathcal{M}) \right] dt + \sqrt{\beta(t)}d\tilde{\mathcal{W}}, \quad (2)$$

where $s(\mathcal{M})$ is the unknown score function and $d\tilde{\mathcal{W}}$ is reverse-time Brownian noise. We design a network that approximates the score function, $s_\theta(\mathcal{M}|t)$, given a material and a time conditioning $t \in [0, 1]$ and will refer to this as the denoiser-network. By training the denoiser-network it intuitively allows for optimization of the likelihood of a material by following the reverse SDE during sampling. The denoiser-network, $s_\theta(\mathcal{M}|t)$, is trained by predicting the vectorial noise added at any given time, t , through denoising score-matching[46] as indicated in Fig. 1(a). The architecture of the denoiser-network is a time-conditioned non-conservative vector-field regressor

implemented using the equivariant PaiNN [41] architecture.

During training a mini-batch of noisy materials is sampled following the known forward diffusion process and a positional score-loss is calculated by taking into account periodic boundary conditions.[28] For the z -direction perpendicular to the substrate surface, we use a truncated Gaussian distribution, while we use a standard Gaussian distribution in the periodic directions. This is illustrated in Fig. 1(b) along with the notion of masked substrate atoms, that are kept fixed throughout the diffusion process. Masking substrate atoms is key when studying surface systems as the substrate is often experimentally known, whereas the overlayer is what dictates the physical and chemical properties.[47] In previous work[30], the substrate interactions have been neglected and therefore does not allow for discovery of peculiar bonding patterns dictated by the underlying surface. The z -confinement serves the purpose that the overlayer only forms on one side of the slab. Sampling materials from a diffusion model consists of following the reversed diffusion process described by Eq. 2 with $s = s_\theta$, starting from the known limiting noise distribution, which in our case is a uniform distribution of atom positions. The time-variable, $t \in \{1, \dots, 0\}$, is discretized in N steps of step-length Δt and a time-annealing is performed such that the time-conditioning of the denoiser-network is reduced for each sampling step. During sampling the Brownian noise in the periodic directions is in the form of Gaussian noise whereas in the z -direction a truncated Gaussian distribution is used such that the atoms never leave the non-periodic confinement. After each sampling step the atoms are wrapped into the periodic cell. We introduce force-field-guidance inspired by classifier-guidance for image generation[48], where the force-prediction of a MLFF, $f(\mathcal{M})$, is gradually introduced during the sampling process in order to guide the reversed diffusion towards more stable materials. The force injection is controlled by the scalar function $\tau(t)$ as

$$d\hat{\epsilon} = \tau(t)f(\mathcal{M})dt, \quad (3)$$

where $\tau(t) = \eta(1 - t)$ with η a constant and $f(\mathcal{M}) = -\nabla_{\mathbf{R}}E(\mathcal{M})$. $d\hat{\epsilon}$ represents an additional term in the reversed diffusion process defined by Eq. 2. This means that, as time is decreasing during sampling, more emphasis is put onto decreasing the predicted force. Furthermore, we include a short local relaxation in the MLFF with step length $\eta\Delta t$ following generation in the potential guidance procedure.

To generate training data for the diffusion model we perform RSS for a number of stoichiometries ranging from Ag_4O_2 to Ag_6O_5 on $\text{Ag}(111)$ within a $c(2 \times 8)$ unit cell. An example of the cell and a training example is presented in Fig. 2(a). RSS provides an unbiased sampling of low energy configurations and is therefore used for generating training data. A total of 22,090

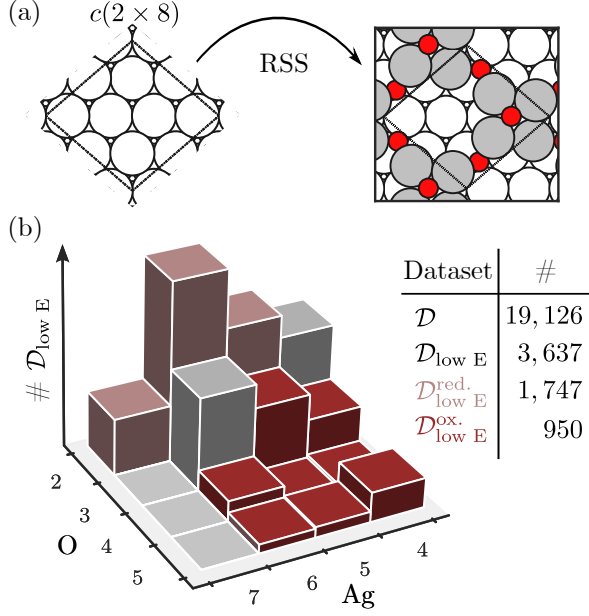


FIG. 2. (a) Training data generation process by performing RSS in the $c(2 \times 8)$ unit cell. (b) Distribution of training data per stoichiometry for the $\mathcal{D}_{\text{low E}}$ dataset. The coloring corresponds to the stoichiometry based split of data with the darker red representing more oxygen and the lighter red represented less oxygen as compared to Ag_2O . A table of dataset names and number of training data is provided as well.

training materials are generated using RSS which are further divided into subsets to investigate model dependence on training data. The data-subsets are presented in Fig. 2(b) showing distribution of stoichiometries for the $\mathcal{D}_{\text{low E}}$ dataset together with the number of training data for each dataset. \mathcal{D} is comprised of all data within 2 eV of the global minimum for each stoichiometry and represents almost all RSS generated materials. Likewise, $\mathcal{D}_{\text{low E}}$ is all data within 0.5 eV of the global minimum for each stoichiometry. A large overweight of reduced compared to oxidized materials are present in this dataset as shown in Fig. 2(b). $\mathcal{D}_{\text{low E}}^{\text{red.}}$ and $\mathcal{D}_{\text{low E}}^{\text{ox.}}$ are the low and high oxygen content subsets of $\mathcal{D}_{\text{low E}}$ as compared to a 2 : 1 silver-oxygen ratio. Each model is trained independently on the respective dataset with $\beta_{\text{min}} = 0.01$ and $\beta_{\text{max}} = 3$ and a representation cutoff of 6\AA in the PaiNN representation. The respective models will be referred to by their training dataset name.

A total of 960 materials are generated for Ag_6O_3 in the slightly larger $p(3 \times 3)$ using each of the four models with potential guidance hyperparameter η chosen such that $\eta\Delta t = 0.001 \text{ \AA eV}^{-1}$. After generation each surface material is relaxed using DFT to be able to compare to RSS.

Fig. 3(a) shows the energy of materials sampled with the \mathcal{D} model as compared to full DFT RSS performed

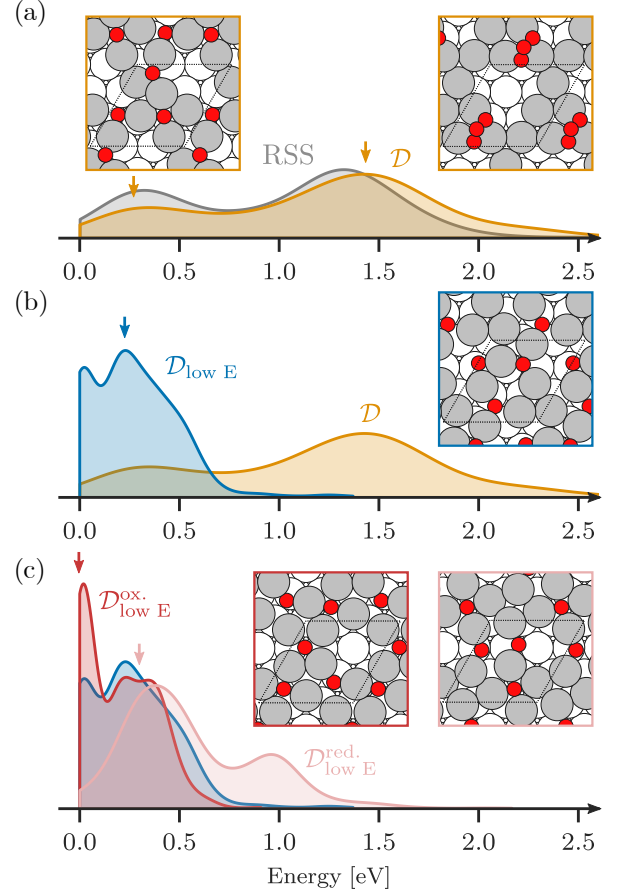


FIG. 3. Energy distributions of generated materials for Ag_6O_3 in a $p(3 \times 3)$ cell for different training dataset selections with RSS as an unbiased benchmark. (a) shows the materials generated by the \mathcal{D} model that highly resembles the energy distribution of RSS. The $\mathcal{D}_{\text{low E}}$ model is able to produce much more stable materials compared to \mathcal{D} as shown in (b). It is possible to bias generation to favor or disfavor the global minimum-energy material by using the $\mathcal{D}_{\text{low E}}^{\text{ox.}}$ model or $\mathcal{D}_{\text{low E}}^{\text{red.}}$ model respectively as presented in (c). Example materials are shown as generated by the different models with corresponding energies indicated by colored arrows.

for the slightly larger test system of Ag_6O_3 in a $p(3 \times 3)$ cell. It is notable that the \mathcal{D} model is able to reproduce the energy distribution of RSS showcasing a similarly unbiased generation across the entire configuration space. Two examples of generated materials are shown from each of the high-likelihood areas. Both feature recognizable bonding motifs with the more stable material displaying triangular and square motifs and the less stable generating a defected $\text{Ag}(111)$ surface with adsorbed ozone. It should be noted that the number of relaxation steps needed with DFT is approximately halved for diffusion generated structures compared to RSS significantly reducing the computation cost. By only training on more stable materials, as is done with the $\mathcal{D}_{\text{low E}}$

model, the energy distribution of generated materials is shifted towards more stable materials as presented in Fig. 3(b). This is a remarkable result, that limiting the training data to low energy materials for a smaller systems yields a higher likelihood of sampling low energy materials for a larger system owing to the generalizable nature of atomistic systems. Furthermore, it shows the importance of choosing a training dataset that compromises between exploration of the entire configurational space of stable materials versus biasing the generation towards the most stable materials. The use of force-field guidance improved the initially generated materials by 2.5 eV on average for the $\mathcal{D}_{\text{low E}}$ model compared to not using force-field guidance. A slightly excited example material is presented in Fig. 3(b) generated by the $\mathcal{D}_{\text{low E}}$ model showing a rotated silver four-ring that highly resembles the most stable materials in the smaller cell of the training data. Furthermore, one can bias the generation by only including specific stoichiometries in the training dataset as shown in Fig. 3(c). The $\mathcal{D}_{\text{low E}}^{\text{ox}}$ model results in an even higher sampling of low energy materials as compared to the $\mathcal{D}_{\text{low E}}$ model, but this effect can not necessarily be deduced a priori. Naturally, if low energy materials for a test system all feature a certain motif that is only present in a subset of the data, one can increase the likelihood of generating such motifs by sub-sampling the training data. Contrary, the $\mathcal{D}_{\text{low E}}^{\text{red}}$ model heavily decreases the likelihood of generating the lowest energy materials. The example material shown for the $\mathcal{D}_{\text{low E}}^{\text{ox}}$ model is the global minimum-energy structure for this choice of cell and stoichiometry. The example material for the $\mathcal{D}_{\text{low E}}^{\text{red}}$ model is less stable, but the generative model is still able to produce motifs that are likely to be stable and could prove valuable to investigate in a high-throughput setting. It is evident that the choice of training data plays an important role when training diffusion models as the generated samples are sampled where the training data likelihood is large. The ability to bias generation provides a major improvement over data agnostic approaches such as RSS along with the computational benefits. Other guidance approaches such as classifier-free guidance[49] could prove beneficial for more controllable generational bias.

The generation-time for diffusion models is directly proportional to the number of discretization steps, N , of the time-conditioning. A finer discretization will lead to a better solution of the reverse SDE, but at a higher computation cost. To investigate the effect of the number of sampling steps on the quality of generated materials, we consider the more demanding Ag_{12}O_6 in the $p(4 \times 4)$ cell with the global minimum-energy surface phase identified as the “Ag₆ model”[50, 51]. The experimental scanning tunneling microscopy images were initially explained with a Ag_{11}O_6 stoichiometry and it took six years to come up with the “Ag₆ model” of the surface phase by means of human intuition. Here, we show our diffusion

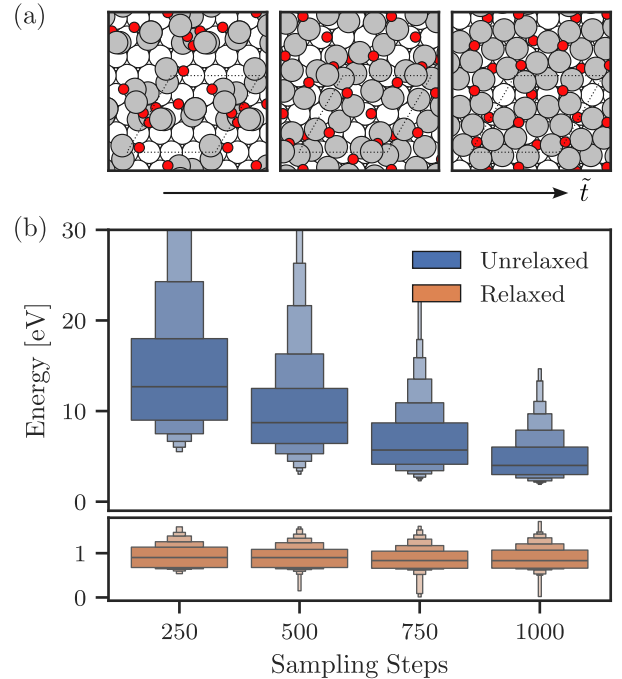


FIG. 4. (a) Structure of material at initial, middle and final step of sampling resulting in the “Ag₆ model”. \hat{t} represents the direction of reversed time during the sampling process. (b) Energy of generated materials for Ag_{12}O_6 in a $p(4 \times 4)$ cell evaluated with DFT before and after DFT relaxation as a function of diffusion steps taken during the sampling procedure.

model is able to identify the novel surface phase removed from human intuition while only having learnt on training data from the much smaller $c(2 \times 8)$ unit cell.

To stabilize the denoiser-network when considering many more atoms than present in the training data, we perform data-augmentation by repeating the training data periodically, such that the effective number of atoms in the training data materials increases. This allows the denoiser-network to learn interactions between a higher number of atoms at no cost of calculating additional training data for larger cells. This data-augmentation technique can equally well be used for bulk materials and ensures stability of the denoiser-network when many atoms are close.

Fig. 4(a) shows the initial, middle and final material during a sampling path. In the initial material, each atom position is drawn from a uniform distribution and thus represents a completely random structure. In the middle of sampling, corresponding to step $t = 0.5$, the material is clearly more ordered with local motifs starting to resemble chemically stable bonding patterns. The final material represents the “Ag₆ model” of silver-oxide on Ag(111) with a central ring, that exposes a substrate atom. We observe that the surface registry is found directly by including the masked substrate atoms in the

diffusion process. Fig. 4(b) shows the distribution of material energies calculated with DFT as a function of the number of diffusion steps used during sampling. In addition the DFT relaxed energies are shown for each number of diffusion steps. The diffusion model is able to generate more stable materials by increasing the number of diffusion steps, but the improvement in stability is achieved primarily by better local optimizations rather than better configurations as is evident from the very similar post-relaxation energies for all choices of diffusion steps. Naturally, it can be advantageous to perform a higher number of sampling steps in order to reduce the computational cost of later ab-initio calculations.

In conclusion, we have introduced a generative diffusion model for surface material discovery that is capable of recovering the “Ag₆ model” of silver-oxide on Ag(111) when trained on small AgO surface materials. We have shown the effect of training data selection on generation performance, where we are able to bias the sampling towards more stable materials. Furthermore, we have shown the importance of the number of diffusion sampling steps in order to obtain chemically stable materials directly from the model. As a future step, this algorithm should be employed for the discovery of previously unknown materials that could be verified experimentally.

We acknowledge support by VILLUM FONDEN through Investigator grant, project no. 16562, and by the Danish National Research Foundation through the Center of Excellence “InterCat” (Grant agreement no: DNRF150). This research was undertaken thanks in part to funding provided to the University of Toronto’s Acceleration Consortium from the Canada First Research Excellence Fund CFREF-2022-00042. AAG thanks Anders G. Frøseth for his generous support. AAG also acknowledges the generous support of Natural Resources Canada and the Canada 150 Research Chairs program.

REFERENCES

- [1] Z. Yao, Y. Lum, A. Johnston, L. M. Mejia-Mendoza, X. Zhou, Y. Wen, A. Aspuru-Guzik, E. H. Sargent, and Z. W. Seh, *Nat Rev Mater* **8**, 202 (2023).
- [2] R. Gómez-Bombarelli, J. N. Wei, D. Duvenaud, J. M. Hernández-Lobato, B. Sánchez-Lengeling, D. Sheberla, J. Aguilera-Iparraguirre, T. D. Hirzel, R. P. Adams, and A. Aspuru-Guzik, *ACS Cent. Sci.* **4**, 268 (2018).
- [3] J. Lim, S. Ryu, J. W. Kim, and W. Y. Kim, *Journal of Cheminformatics* **10**, 31 (2018).
- [4] Q. Liu, M. Allamanis, M. Brockschmidt, and A. Gaunt, in *Advances in Neural Information Processing Systems*, Vol. 31 (Curran Associates, Inc., 2018).
- [5] W. Jin, R. Barzilay, and T. Jaakkola, in *Proceedings of the 35th International Conference on Machine Learning* (PMLR, 2018) pp. 2323–2332.
- [6] J. Noh, J. Kim, H. S. Stein, B. Sanchez-Lengeling, J. M. Gregoire, A. Aspuru-Guzik, and Y. Jung, *Matter* **1**, 1370 (2019).
- [7] Z. Yao, B. Sánchez-Lengeling, N. S. Bobbitt, B. J. Bucior, S. G. H. Kumar, S. P. Collins, T. Burns, T. K. Woo, O. K. Farha, R. Q. Snurr, and A. Aspuru-Guzik, *Nat Mach Intell* **3**, 76 (2021).
- [8] B. Kim, S. Lee, and J. Kim, *Science Advances* **6**, eaax9324 (2020).
- [9] T. Long, N. M. Fortunato, I. Opahle, Y. Zhang, I. Samathrakakis, C. Shen, O. Gutfleisch, and H. Zhang, *npj Comput Mater* **7**, 1 (2021).
- [10] Y. Zhao, M. Al-Fahdi, M. Hu, E. M. D. Siriwardane, Y. Song, A. Nasiri, and J. Hu, *Advanced Science* **8**, 2100566 (2021).
- [11] M. Alverson, S. G. Baird, R. Murdock, E. Sin-Hang Ho, J. Johnson, and T. D. Sparks, *Digital Discovery* **3**, 62 (2024).
- [12] N. Gebauer, M. Gastegger, and K. Schütt, in *Advances in Neural Information Processing Systems*, Vol. 32 (Curran Associates, Inc., 2019).
- [13] C. Shi, M. Xu, Z. Zhu, W. Zhang, M. Zhang, and J. Tang, “GraphAF: A Flow-based Autoregressive Model for Molecular Graph Generation,” (2020), arxiv:2001.09382 [cs, stat].
- [14] J. Westermayr, J. Gilkes, R. Barrett, and R. J. Maurer, *Nat Comput Sci* **3**, 139 (2023).
- [15] M. S. Jørgensen, H. L. Mortensen, S. A. Meldgaard, E. L. Kolsbjerg, T. L. Jacobsen, K. H. Sørensen, and B. Hammer, *The Journal of Chemical Physics* **151** (2019).
- [16] G. Simm, R. Pinsler, and J. M. Hernandez-Lobato, in *Proceedings of the 37th International Conference on Machine Learning* (PMLR, 2020) pp. 8959–8969.
- [17] S. A. Meldgaard, J. Köhler, H. L. Mortensen, M.-P. V. Christiansen, F. Noé, and B. Hammer, *Mach. Learn.: Sci. Technol.* **3**, 015008 (2021).
- [18] J. Yoon, Z. Cao, R. K. Raju, Y. Wang, R. Burnley, A. J. Gellman, A. B. Farimani, and Z. W. Ulissi, *Mach. Learn.: Sci. Technol.* **2**, 045018 (2021).
- [19] L. A. Thiede, M. Krenn, A. Nigam, and A. Aspuru-Guzik, *Mach. Learn.: Sci. Technol.* **3**, 035008 (2022).
- [20] R. Barrett and J. Westermayr, *J. Phys. Chem. Lett.* **15**, 349 (2024).
- [21] D. Flam-Shepherd, K. Zhu, and A. Aspuru-Guzik, *Nat Commun* **13**, 3293 (2022).
- [22] N. Fu, L. Wei, Y. Song, Q. Li, R. Xin, S. S. Omeo, R. Dong, E. M. D. Siriwardane, and J. Hu, *Mach. Learn.: Sci. Technol.* **4**, 015001 (2023).
- [23] L. M. Antunes, K. T. Butler, and R. Grau-Crespo, “Crystal Structure Generation with Autoregressive Large Language Modeling,” (2024), arxiv:2307.04340 [cond-mat].
- [24] C. Zang and F. Wang, in *Proceedings of the 26th ACM SIGKDD International Conference on Knowledge Discovery & Data Mining*, KDD ’20 (Association for Computing Machinery, New York, NY, USA, 2020) pp. 617–626.
- [25] M. Kuznetsov and D. Polykovskiy, *Proceedings of the AAAI Conference on Artificial Intelligence* **35**, 8226 (2021).
- [26] C. Ma and X. Zhang, in *Proceedings of the 30th ACM International Conference on Information & Knowledge*

- Management*, CIKM '21 (Association for Computing Machinery, New York, NY, USA, 2021) pp. 1181–1190.
- [27] J. Köhler, M. Invernizzi, P. de Haan, and F. Noé, “Rigid Body Flows for Sampling Molecular Crystal Structures,” (2023), arxiv:2301.11355 [physics, stat].
 - [28] T. Xie, X. Fu, O.-E. Ganea, R. Barzilay, and T. Jaakkola, “Crystal Diffusion Variational Autoencoder for Periodic Material Generation,” (2022), arxiv:2110.06197 [cond-mat, physics:physics].
 - [29] E. Hoogetboom, V. G. Satorras, C. Vignac, and M. Welling, “Equivariant Diffusion for Molecule Generation in 3D,” (2022), arxiv:2203.17003 [cs, q-bio, stat].
 - [30] P. Lyngby and K. S. Thygesen, npj Comput Mater **8**, 1 (2022).
 - [31] V. Fung, S. Jia, J. Zhang, S. Bi, J. Yin, and P. Ganesh, Mach. Learn.: Sci. Technol. **3**, 045018 (2022).
 - [32] B. Jing, G. Corso, J. Chang, R. Barzilay, and T. Jaakkola, “Torsional Diffusion for Molecular Conformer Generation,” (2023), arxiv:2206.01729 [physics, q-bio].
 - [33] Y. Zhao, E. M. D. Siriwardane, Z. Wu, N. Fu, M. Al-Fahdi, M. Hu, and J. Hu, npj Comput Mater **9**, 1 (2023).
 - [34] T. Weiss, E. Mayo Yanes, S. Chakraborty, L. Cosmo, A. M. Bronstein, and R. Gershoni-Poranne, Nat Comput Sci, 1 (2023).
 - [35] C. Zeni, R. Pinsler, D. Zügner, A. Fowler, M. Horton, X. Fu, S. Shysheya, J. Crabbé, L. Sun, J. Smith, R. Tomioka, and T. Xie, “MatterGen: A generative model for inorganic materials design,” (2023), arxiv:2312.03687 [cond-mat].
 - [36] H. Moustafa, P. M. Lyngby, J. J. Mortensen, K. S. Thygesen, and K. W. Jacobsen, Phys. Rev. Mater. **7**, 014007 (2023).
 - [37] X. Fu, T. Xie, A. S. Rosen, T. Jaakkola, and J. Smith, “MOFDiff: Coarse-grained Diffusion for Metal-Organic Framework Design,” (2023), arxiv:2310.10732 [cond-mat, physics:physics].
 - [38] A. Cheng, A. Lo, S. Miret, B. Pate, and A. Aspuru-Guzik, “Reflection-Equivariant Diffusion for 3D Structure Determination from Isotopologue Rotational Spectra in Natural Abundance,” (2023), arxiv:2310.11609 [astro-ph, physics:physics].
 - [39] R. Elijošius, F. Zills, I. Batatia, S. W. Norwood, D. P. Kovács, C. Holm, and G. Csányi, “Zero Shot Molecular Generation via Similarity Kernels,” (2024), arxiv:2402.08708 [physics].
 - [40] N. Thomas, T. Smidt, S. Kearnes, L. Yang, L. Li, K. Kohlhoff, and P. Riley, “Tensor field networks: Rotation- and translation-equivariant neural networks for 3D point clouds,” (2018), arxiv:1802.08219 [cs].
 - [41] K. Schütt, O. Unke, and M. Gastegger, in *Proceedings of the 38th International Conference on Machine Learning* (PMLR, 2021) pp. 9377–9388.
 - [42] J. Gastegger, F. Becker, and S. Günnemann, in *Advances in Neural Information Processing Systems*, Vol. 34 (Curran Associates, Inc., 2021) pp. 6790–6802.
 - [43] S. Batzner, A. Musaelian, L. Sun, M. Geiger, J. P. Mailoa, M. Kornbluth, N. Molinari, T. E. Smidt, and B. Kozinsky, Nat Commun **13**, 2453 (2022).
 - [44] C. J. Pickard and R. J. Needs, J. Phys.: Condens. Matter **23**, 053201 (2011).
 - [45] Y. Song, J. Sohl-Dickstein, D. P. Kingma, A. Kumar, S. Ermon, and B. Poole, “Score-Based Generative Modeling through Stochastic Differential Equations,” (2021), arxiv:2011.13456 [cs, stat].
 - [46] Y. Song and S. Ermon, in *Advances in Neural Information Processing Systems*, Vol. 32 (Curran Associates, Inc., 2019).
 - [47] H. Li, Y. Jiao, K. Davey, and S.-Z. Qiao, Angewandte Chemie **135**, e202216383 (2023).
 - [48] P. Dhariwal and A. Nichol, “Diffusion Models Beat GANs on Image Synthesis,” (2021), arxiv:2105.05233 [cs, stat].
 - [49] J. Ho and T. Salimans, “Classifier-Free Diffusion Guidance,” (2022), arxiv:2207.12598 [cs].
 - [50] J. Schnadt, A. Michaelides, J. Knudsen, R. T. Vang, K. Reuter, E. Lægsgaard, M. Scheffler, and F. Besenbacher, Phys. Rev. Lett. **96**, 146101 (2006).
 - [51] M. Schmid, A. Reicho, A. Stierle, I. Costina, J. Klikovits, P. Kostelnik, O. Dubay, G. Kresse, J. Gustafson, E. Lundgren, J. N. Andersen, H. Dosch, and P. Varga, Phys. Rev. Lett. **96**, 146102 (2006).